Electronic Supplementary Material (ESI) for Analyst.

Chemiluminescence Resonance Energy Transfer-Based Multistage Nucleic Acid Amplification Circuit for MiRNA Detection with Low Background

Nana Kang,[a] Benrui Weng,[a] Sijia Liu,[a] Huiran Yang,[a] Siyuan Wang,[a] Yaqi Liu,[a] Jiabing Ran,[a] Hanghang Liu,[a] Zhangshuang Deng,[a] Changying Yang,[a] Huimin Wang,*[a] Fuan Wang [b]

[a] Hubei Key Laboratory of Natural Products Research and Development, College of Biological and Pharmaceutical Sciences, China Three Gorges University, Yichang, Hubei 443002 (P. R. China). E-mail: hmwang@ctgu.edu.cn.

[b] College of Chemistry and Molecular Sciences, Wuhan University, Wuhan, Hubei 430000 (P. R. China).

Table of Contents

Experimental Section

Instrumentation

Shimadzu UV-2600 was used to detect the absorption of hemin and DNA. Edinburgh Instruments Spectrofluorometer FS5 was used for the detection of the fluorescence of luminol and Ce6. PCR and Gel imager were purchased from BIO-RAD. The ultra-weak chemiluminescence analyzer BPCL-1-TIC with a 600 nm filter was used to detect the luminescence of Ce6. CLSM images were collected via confocal laser scanning microscopy (A1R+, Nikon, Japan). AFM was purchased from Bruker.

Cell culture

MCF-7 cells were cultured in a 1640 medium containing fetal bovine serum (10%) and penicillin (1%) at 37°C in a CO_2 incubator. Hela cells were cultured in a DMEM medium containing fetal bovine serum (10%) and penicillin (1%) and MCF-10A were cultured in the special medium for MCF-10A cells at 37°C in a CO_2 incubator.

Cytotoxicity assay

3-(4,5-dimethylthiazol-2)-2,5-diphenyltetrazole bromide (MTT) the reagent was used to test the cell viability with different treatments. MCF-7 cells were inoculated on a 96-well plate at a density of 1×10^5 cells per well for 24 h. Different concentrations of hairpins were transfected into cells by liposome and incubated for 48 hours. Hemin, luminol, and H_2O_2 are directly added. 20 μL of MTT (5 mg/mL) reagent were added to each well and incubated at 37°C for 4 h. Finally, the MTT solution was carefully removed. 150 μL of DMSO was added to each well, and the 96-well plate was gently shaken at room temperature for 10 min. The cytotoxicity of the materials was analyzed by a microplate reader (BIO-RAD) at 490 nm.

Atomic force microscopy (AFM) imaging

$MgCl_2$ (10 mM) was deposited on a freshly cleaved mica surface for 2 min, followed by its rinsing with ultrapure water and drying under a stream of nitrogen. 0.33 μM H1,

0.33 μM H2, 0.66 μM H3, 0.66 μM H4, 0.66 μM H5, and 0.66 μM H6 were reacted with 100 nM I in 10 mM HEPES buffer at 37℃ for 12 h. The resulting CHA-HCR-DNAzyme products were diluted to 20 nM with 10 mM HEPES buffer and then deposited on the mica surface. Photographed by Multimode-8 AFM.

Polyacrylamide gel electrophoresis analysis

12% polyacrylamide gel was prepared and 0.5×TBE buffer was added, then the prepared sample was injected into the gel. The reaction time was about 2 h at a room temperature of 100 V. Finally, the gel was removed and soaked in Gel-Red for about 15 min. The images were collected by Gel Doc EZ imager.

Table S1. Sequences of nucleic acid molecules involved in the text

No.	Sequence (5'→3')
H1	CTC TAT CAT TAT CTT GCT TCA TCT TCA TCA AGA TAA TGA TAG AGA CCG ACA CTC
H2	GCT TCA TCT TCA TCT TCT CTA TCA TTA TCT TGA TGA AGA TGA AGC AAG ATA AT
H3	GAG TGT CGG AGA TGA AGA TGA AGC CAT CGT GCT TCA TCT TCA TCT CCG TGG GTA GGG CG
H3-1	GAG TGT CGG AGA TGA AGA TGA AGC CAT CGT GCT TCA TCT TCA TCT CCG TGG GTA GGG CGG
H3-2	GAG TGT CGG AGA TGA AGA TGA AGC CAT CGT GCT TCA TCT TCA TCT CCG TGG GTA GGG C
H4	Ce6-GCT TCA TCT TCA TCT CCG GTT TTG CGG AGA TGA AGA TGA AGC ACG ATG
Without Ce6-H4	GCT TCA TCT TCA TCT CCG GTT TTG CGG AGA TGA AGA TGA AGC ACG ATG
H5	G GTG GGT CAA AAC CGG AGA TGA AGA TGA AGC TTG CCT GCT TCA TCT TCA TCT CCG
H5-1	GTG GGT CAA AAC CGG AGA TGA AGA TGA AGC TTG CCT GCT TCA TCT TCA TCT CCG
H5-2	GG GTG GGT CAA AAC CGG AGA TGA AGA TGA AGC TTG CCT GCT TCA TCT TCA TCT CCG
H6	GCT TCA TCT TCA TCT CCG ACA CTC CGG AGA TGA AGA TGA AGC AGG CAA
H7	TCA ACA TCA GTC TGA TAA GCT AAG AGT GTC GGT CTC TAT CAT TAT CTT AGC TTA TCA GAC TGA T
I	GAG TGT CGG TCT CTA TCA TTA TCT T
T	GCT TCA TCT TCA TCT CCG ACA CTC
MiRNA-21	UAG CUU AUC AGA CUG AUG UUG A
Let-7a miRNA	UGA GGU AGU AGG UUG UAU AGU U
MiRNA-141	UAA CAC UGU CUG GUAAAG AUG G
MiRNA-222	AGC UAC AUC UGG CUA CUG GGU CUC
MiRNA-21 inhibitor	AUC GAA UAG UCU GAC UAC AAC U
MiRNA-21mimic	UAG CUU AUC AGA CUG AUG UUG A

The orange part is the split G-quadruplex domain

Table S2. Comparison of different methods for nucleic acid detection

System	Analyte	Detection method	Application system	Linear range (nM)	LOD (nM)	Ref
HCR-MOFs	miRNA	Chemiluminescence	solution	5 -333	1.67	1
DNAzyme/WS_2	miRNA	Chemiluminescence	solution	0.5-10	0.18	2
DNA-grafted Hemin	miRNA	Chemiluminescence	solution	5-50	0.17	3
PDANP/dsDNA	miRNA	Chemiluminescence	solution	0.08-100	0.08	4
CHA-HCR-DNAzyme	miRNA	Chemiluminescence	cells	0.5-20	0.174	This work

The detailed principle of the CD system

These hairpin reactants are metastable without target DNA and can only be activated by their corresponding triggers (domains x and x* are complementary to each other). The CHA-DNAzyme (CD) consists of five hairpins H1, H2, H3, H4, and H5 (**Fig. S1**). H1 includes toehold d*, complementary stem a-b and a*-b*, and ring c*. H2 consists of toehold b*, complementary stem c* and c, and ring a-b. Domain d-a-b of initiator I initiates the opening of H1 through the complementary sequence d*-a*-b* to generate the I-H1 complex and expose a-b-c*. The exposed domain opens H2, yielding the intermediate structure "I-H1·H2". Eventually, initiator I was releases and a lot of dsDNA H1·H2 are produced. The released initiator I continue to participate in the CHA reaction. The generated trigger T can trigger the hybridization of H3, H4, and H5 in sequence, yielding the structure "T-H3·H4·H5" which form recombined DNAzyme.

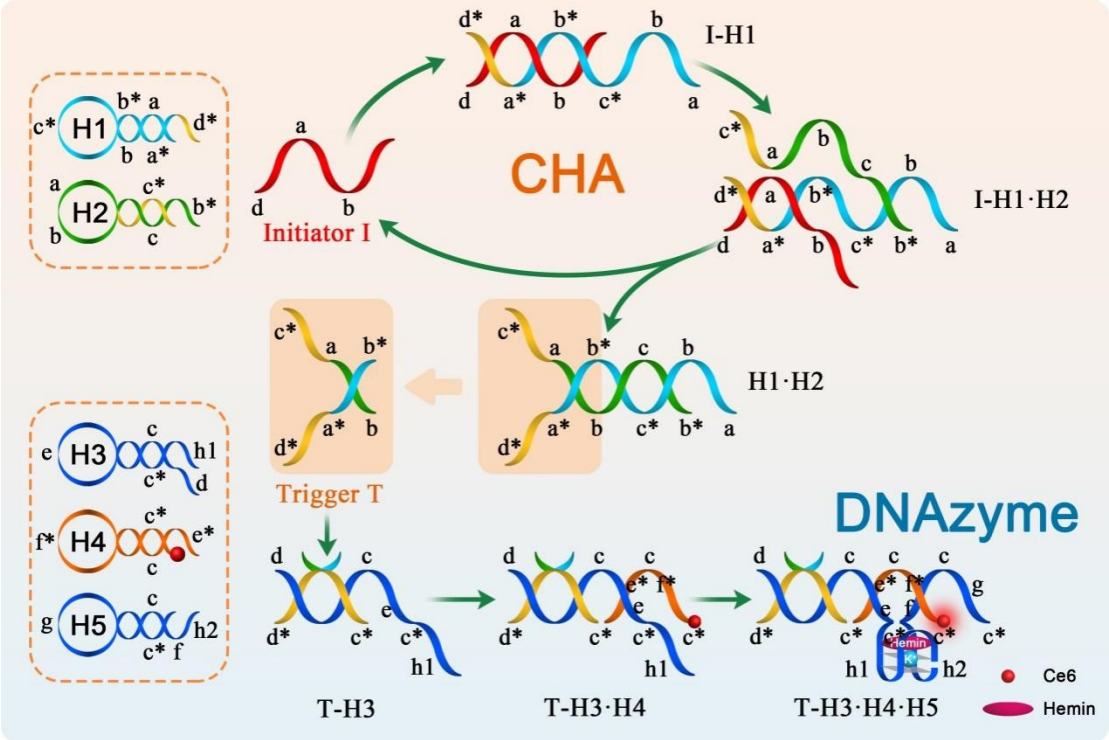

Fig. S1 Schematic diagram of CHA-DNAzyme (CD) system.

The detailed principle of the HD system

The HCR-DNAzyme (HD) consists of four hairpins H3, H4, H5, and H6 (**Fig. S2**). H3 includes toehold h1, complementary stem c and c*, ring e, and overhang d. H4 consists of toehold e*, complementary stem c* and c, and ring f*. H5 consists of complementary stem c* and c, ring g, and overhang f-h2. h1 and h2 are two parts of the G-quadruplex. H6 includes toehold g*, complementary stem c* and c, and ring d*. The target "T" can open H3 to produce the intermediate "T-H3". Domain e-c* hybridizes with domain c-e* of H4 and opens H4 to yield structure "T-H3·H4". The resulting structure "T-H3·H4" hybridizes with domain f-c of H5, yielding structure "T-H3·H4·H5". The exposed g and c* hybridize with H6, yielding structure "T-H3·H4·H5·H6" and expose the same sequence as T to initiated the assembly of H3, H4, H5, and H6 for the HD system.

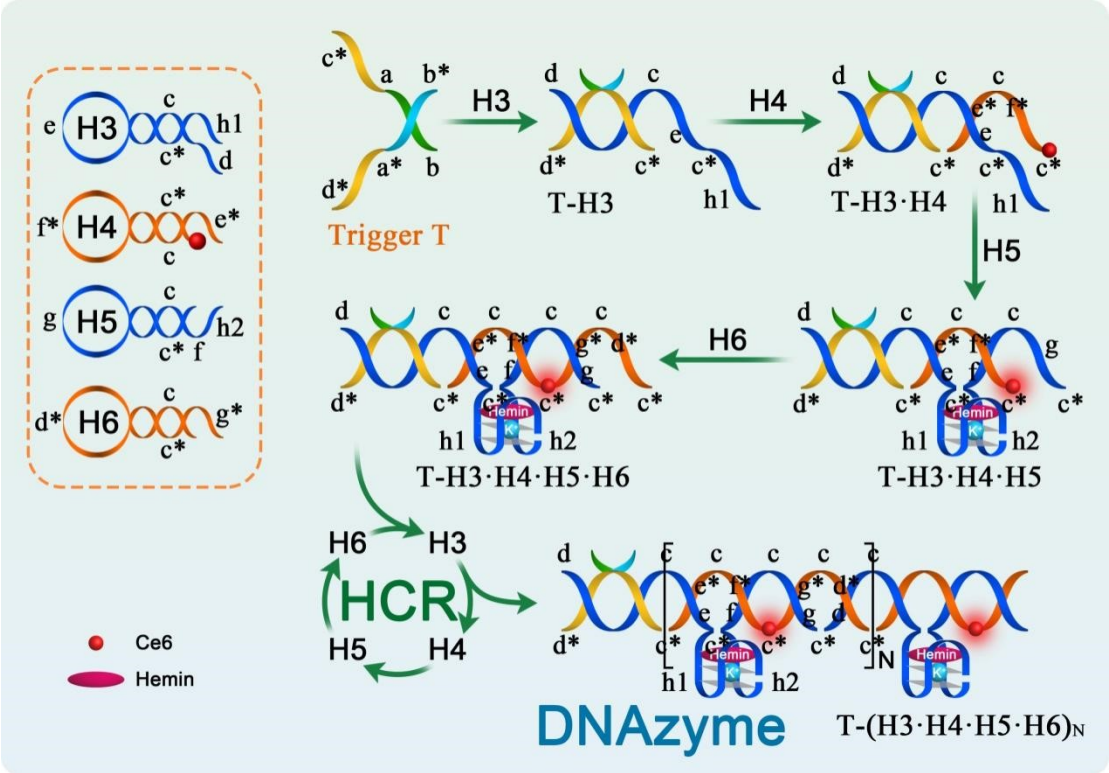

Fig. S2 Schematic diagram of HCR-DNAzyme (HD) system.

Polyacrylamide gel electrophoresis analysis

As shown in **Fig. S3**, the hybridization process of CHA-HCR-DNAzyme can be analyzed. When there was no target for CHA (lane g), HCR (lane i), and CHA-HCR (lane k), the product bands were less, indicating that these hairpin mixtures were metastable and false hybridization could be ignored. In the presence of the target, a large number of DNA bands were observed (lane h, j, l). It was proved that CHA-HCR-DNAzyme hybridization could be successfully carried out.

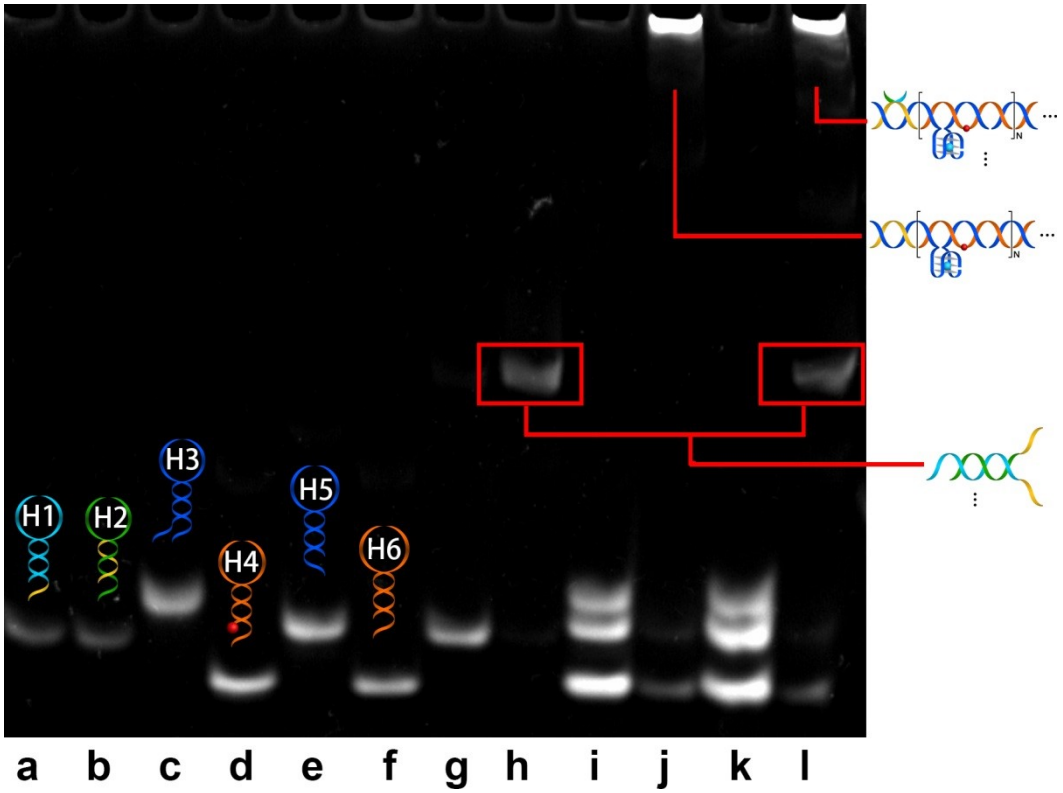

Fig. S3 Polyacrylamide gel electrophoresis. Lanes a to l represent the H1, H2, H3, H4, H5, H6, H1 + H2, H1 + H2 + I, H3 + H4 + H5 + H6, H3 + H4 + H5 + H6 + T, H1 + H2 + H3 + H4 + H5 + H6, and H1 + H2 + H3 + H4 + H5 + H6 + I, respectively. Experimental conditions: 0.33 μM H1, 0.33 μM H2, 0.66 μM H3, 0.66 μM H4, 0.66 μM H5, 0.66 μM H6, without or with I or T of 100 nM.

Atomic force microscopy (AFM) imaging

The morphological features of CHD-assembled nanostructures were characterized by atomic force microscopy (**Fig. S4**). The I-triggered CHD system generated micrometer-long dsDNA nanowires with a height of about 2 nm, while only tiny dots were observed for the non-triggered CHD system, demonstrating the formation of HCR-assembled nanowires and the metastable hairpin components.

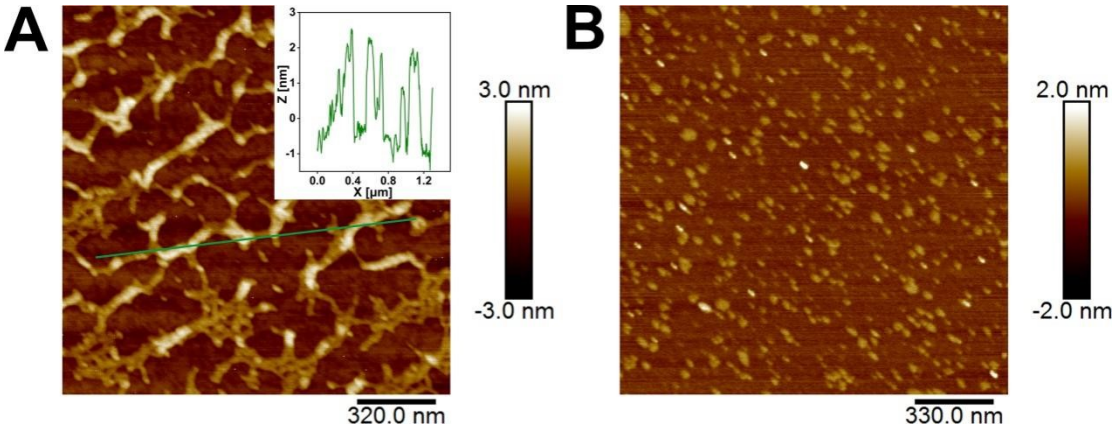

Fig. S4 AFM images of the CHA-HCR-DNAzyme mixture with (A) and without (B) initiator I. Inset: cross-section analysis of the resulting CHA-HCR-DNAzyme nanowires.

The formation of G-quadruplex

To prove that the CHA-HCR-DNAzyme circuit produces G-quadruplexes, we verified that the fluorescence intensity of thioflavin T increased significantly after recombination with G-quadruplexes. Thioflavin T was added to the DNA incubation solution (**Fig. S5**). After co-incubating for 1.5 hours, it was excited at 420 nm and detected by a fluorescence spectrometer, and a significant fluorescence increase at 490 nm was observed.

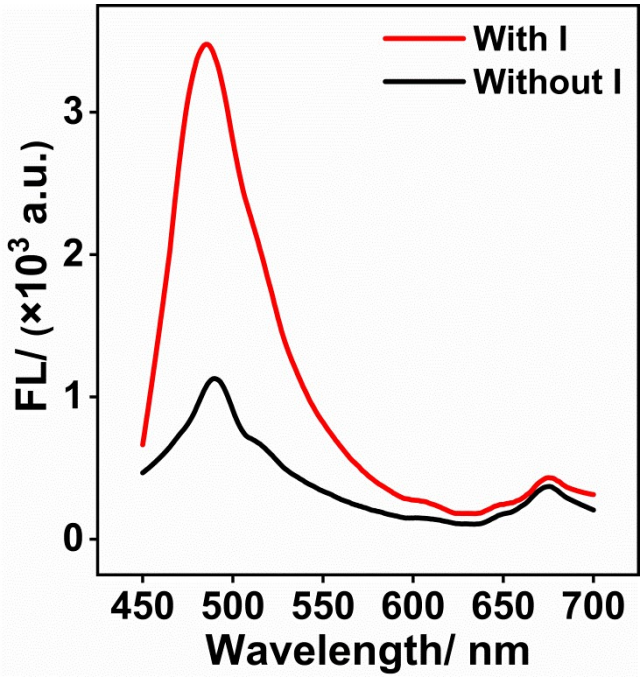

Fig. S5 Fluorescence spectra of the thioflavin T in different solutions. Experimental conditions: 0.33 μM H1, 0.33 μM H2, 0.66 μM H3, 0.66 μM without Ce6-H4, 0.66 μM H5, 0.66 μM H6, without or with initiator I of 100 nM, 0.15 μM thioflavin T, and 10 mM HEPES buffer (pH 6.5, containing 600 mM NaCl, 50 mM KCl, and 10 mM $MgCl_2$).

The conjugation of G-quadruplex with hemin

Hemin was added to the DNA incubation solution for one hour. It has been reported that the binding of hemin and G-quadruplex could induce a red shift and increased intensity of the Soret band of the porphyrin π system of hemin due to different environments for porphyrin.[5] This method has been widely applied to investigate the interaction of hemin and G-quadruplex by absorption titration experiments.[6,7] As shown in **Fig. S6**, in the presence of the target, a complete G-quadruplex was formed, and the UV absorption of hemin increased, proving that hemin successfully combined with the generated G-quadruplex.

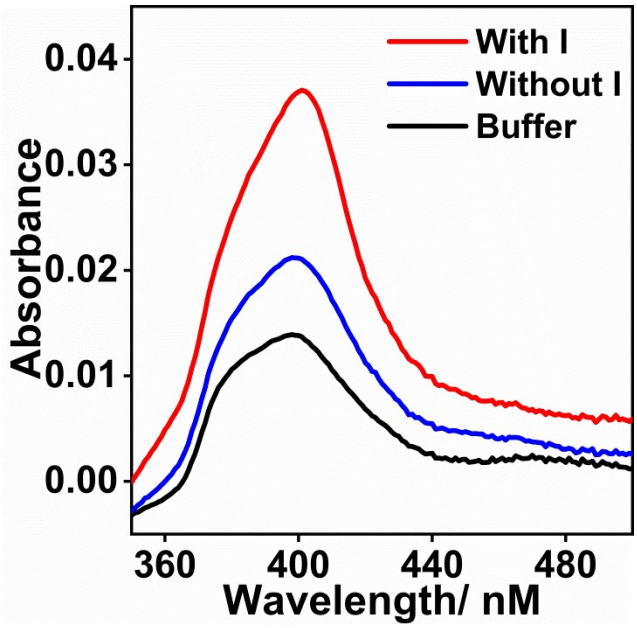

Fig. S6 Absorption spectroscopy of hemin reacted with DNA incubation solution (contain 0.33 μM H1, 0.33 μM H2, 0.66 μM H3, 0.66 μM without Ce6-H4, 0.66 μM H5, 0.66 μM H6, without or with 100 nM I) or buffer. The reaction was carried out in 10 mM HEPES buffer (pH 6.5, containing 600 mM NaCl, 50 mM KCl, and 10 mM $MgCl_2$).

Chemiluminescence spectrum of luminol

In order to verify the feasibility of CRET, the emission spectra of luminol with and without I were tested respectively. As shown in **Fig. S7**, we can observe the emission spectrum of the luminol donor at 425 nm in the presence of initiator.

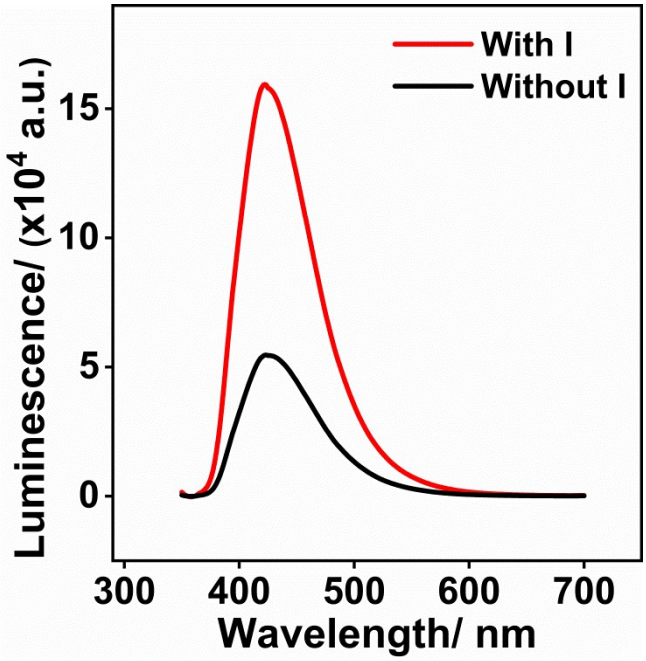

Fig. S7 Chemiluminescence spectra of luminol in the CHD circuit with or without initiator. Experimental conditions: 0.33 μM H1, 0.33 μM H2, 0.66 μM H3, 0.66 μM without Ce6-H4, 0.66 μM H5, 0.66 μM H6, without or with initiator I of 100 nM, 0.15 μM thioflavin T, and 10 mM HEPES buffer (pH 6.5, containing 600 mM NaCl, 50 mM KCl, and 10 mM $MgCl_2$).

Validation of the CRET between luminol and Ce6 fluorophore

The luminol and Ce6 fluorophore were applied as a moderate CRET pair to study the CHD strategy. As shown in **Fig. S8A**, the absorption spectrum of Ce6 fluorophore acceptor has a sufficient spectral overlap with the chemiluminescence emission spectrum of luminol donor, validating the CRET process can proceed from luminol to Ce6. As shown **Fig. S8B**, the distance between adjacent base pairs is about 0.34 nm,[8] the distance between Ce6 and G-quadruplex was calculated to be approximately 8.16 nm with 24 base pairs in CHD product, which was less than 10 nm to ensure the effective CRET process.

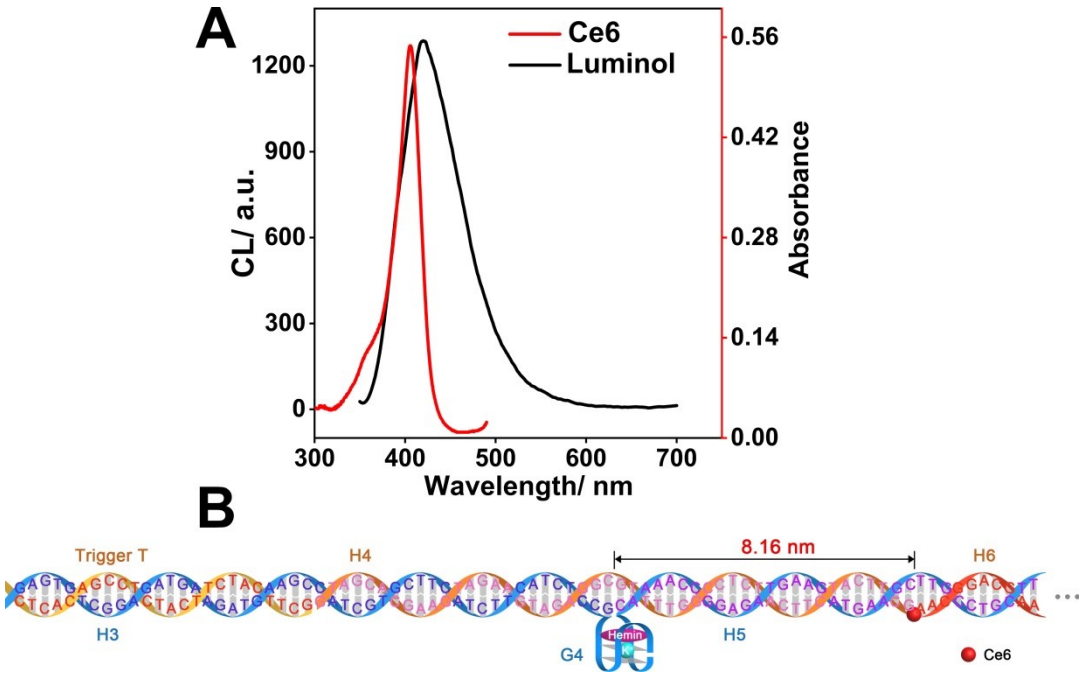

Fig. S8 (A) The chemiluminescence emission spectrum of the donor (luminol) and absorption spectrum of the acceptor (Ce6). There is sufficient spectral overlap between the absorbance of Ce6 and the emission of luminol to enable efficient CRET transduction from luminol to the Ce6 fluorophore. (B) Distance diagram of luminol and Ce6.

DNA-Ce6 and Ce6 Fluorescence Kinetic Curves

The Ce6 is connected to H4 by amide reaction and ordered from Takara (**Fig. S9A**). The Ce6 modified on H4 nucleic acid sequence and free Ce6 were excited at 425 nm, and the fluorescence peak at 672 nm was normalized. It can be seen that within 5 hours, the fluorescence of free Ce6 decreased by about 50%, while the fluorescence of the nucleic acid-linked Ce6 is only reduced by about 10% (**Fig. S9B**). It is proved that the modification of Ce6 on nucleic acid is more beneficial to the hydrophilicity of Ce6, which overcomes the disadvantage of poor dispersion in buffer solution, and is beneficial to the application of Ce6 in buffer solution.

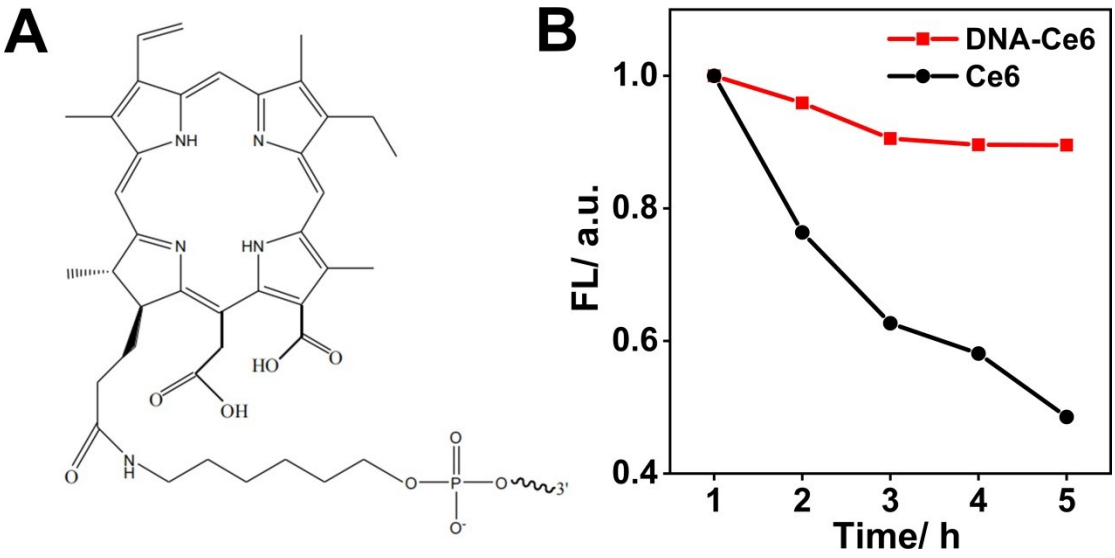

Fig. S9 (A) The linkage of Ce6 on H4. (B) Normalized fluorescence intensity of DNA-Ce6 and Ce6.

Investigation of the energy transfer process

To further investigate the energy transfer process, CHD circuit reactions were performed in the presence and absence of Ce6 on H4 to record the luminol and Ce6 signals in the I-triggered DNA nanowire product, respectively. After the introduction of Ce6, the emission intensity of luminol as the donor decreased at 425 nm (**Fig. S10A**), while the emission peak of Ce6 as the acceptor appeared at 672 nm (**Fig. S10B**). The calculation formula for CRET efficiency is as follows :

$$E_{CRET} = \frac{(S_1 - S_2)}{S_1} \times 100\% = \frac{(14394841.14 - 7411708.96)}{14394841.14} \times 100\% = 48.51\%$$

where S_1 corresponds to the integral area of the luminol emission spectrum generated by the I-initiated circuit in which H4 isn't modified with Ce6, and S_2 corresponds to the integral area of the luminol emission spectrum generated by the I-initiated CHD circuit in which H4 is modified with Ce6 (**Fig. S10A**). So the CRET efficiency of the system is 48.51%.

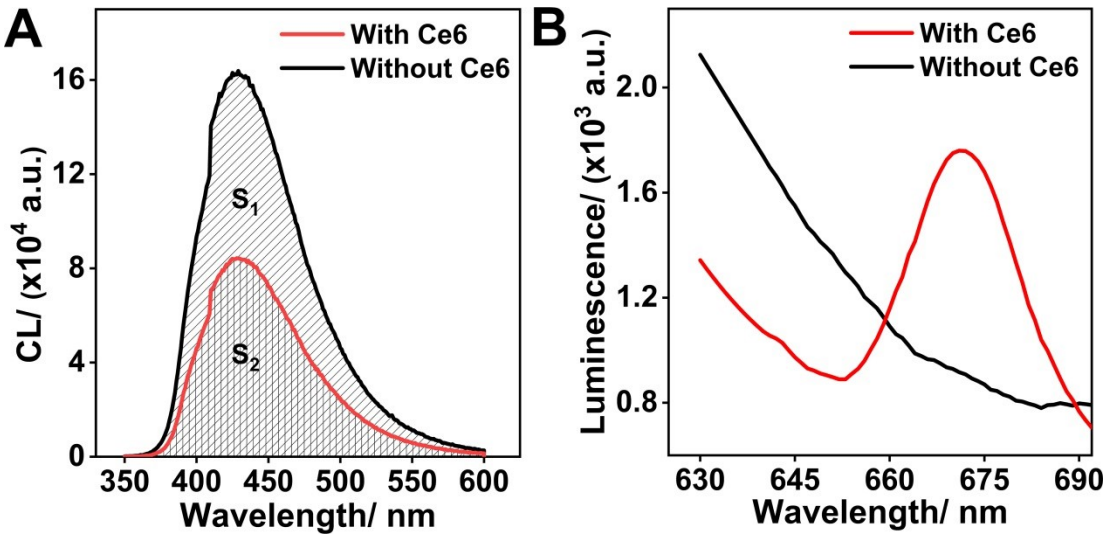

Fig. S10 (A) The emission spectra of luminol were recorded when the I-triggered CHD circuit reaction was performed in the presence and absence of Ce6 on H4, respectively. (B) The emission spectra of Ce6 were recorded when the I-triggered CHD circuit reaction was performed in the presence and absence of Ce6 on H4, respectively.

Optimization of Mg^{2+} concentration and pH

Studies have shown that the introduction of salts such as sodium chloride and magnesium chloride into the annealing solution can greatly reduce the background of CHA while increasing the signal-to-background (S/N) ratio. Therefore, it is necessary to optimize the concentration of Mg^{2+} in the buffer solution for the improving of the detection sensitivity. The S/N ratio of the CHD system showed a 6-fold increase when the concentration of Mg^{2+} increased from 0 to 10 mM because the addition of magnesium chloride to the annealing solution facilitated the formation of correctly folded hairpins which increased the hairpin stability and decreased the background leakage (**Fig. S11A**). While the further increase of magnesium ion concentration from 10 mM to 30 mM led to a significantly increased background signal due to the facilitated hybridization of hairpin reactants in the absence of a target, resulting in a decreased S/N ratio.

pH is an important factor for the catalytic activity of hemin, thus the effect of pH on the S/N ratio was investigated. As shown in **Fig. S11B**, pH decreased from 7.5 to 5.5 leading to the simultaneous decrease of signal and background leakage in the CHD system due to the aggregation of hemin and the decreased catalytic activity of hemin under acidic conditions, while the S/N ratio increased when pH weakened from 7.5 to 6.5 and then decreased slightly at pH 5.5, which might be attributed to the low background leakage of the aggregated hemin and the remained high catalytic activity of G-quadruplex/hemin in the I-initiated CHD circuit under acidic conditions. The Mg^{2+} concentration and pH were optimized to be 10 mM and 6.5, respectively.

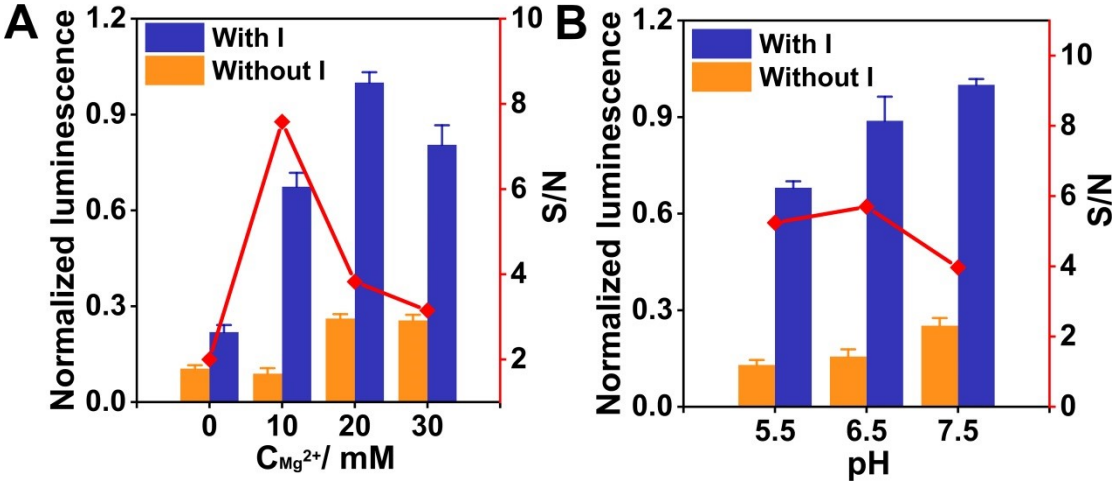

Fig. S11 (A) The Ce6 luminescence intensities of DNA circuits without I or with I at 100 nM under different Mg^{2+} in solution. (B) The Ce6 luminescence intensity of DNA circuits without I or with I at 100 nM at different pH for 12 h.

Optimization of the concentration of CHA/HCR

The concentration of CHA/HCR also plays important role in the generation of the reconstituted G-quadruplex. As a signal read-out part, the relative content of HCR and CHA has an important influence on the DNA circuit. The ratio of CHA/HCR is adjusted by fixing the CHA concentration of 0.33 μM while increasing the HCR concentration to 0.33 μM, 0.66 μM, and 0.99 μM (**Fig. S12**). The chemiluminescence intensity of the I-initiated DNA circuit with I increases with increasing concentration of HCR, while the background increases correspondingly, resulting in decreased S/N ratio. The signal may tend to equilibrate because the CHA/HCR ratio gradually increases and the CHA has all reacted completely, while the remaining H3, H4, H5, and H6 that have not been triggered accumulate in the solution causing background leakage. So the final concentration of CHA/HCR is chosen to be 0.33 μM: 0.66 μM.

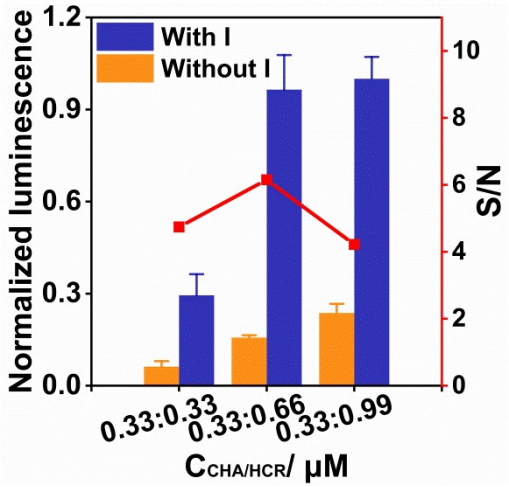

Fig. S12 The Ce6 luminescence intensity of different concentrations of CHA/HCR. The reaction was carried out in 10 mM HEPES buffer (pH 6.5, containing 600 mM NaCl, 50 mM KCl, and 10 mM $MgCl_2$). Results are presented as means ± standard deviation (n = 3).

Optimization of the split G-quadruplex mode

The split G-quadruplex mode is also critical for the generation of G-quadruplex in the absence of a target (**Fig. S13A**). According to our previous work on G-quadruplex mode optimization, the split G-quadruplex mode on H3 and H5 (12:6) was further slightly optimized by transferring the partial G-quadruplex sequence of H3 to that of H5 (11:7 and 10:8). As the G-rich sequence on H5 increased, the signal of I-initiated CHD also raised, and the background maintained with G-quadruplex mode of 11:7 while the background increased significantly with the G-quadruplex mode of 10:8 which might be caused by the self-assembly of half G-quadruplex sequences on H3 or H5 (**Fig. S13B**). Thus G-quadruplex mode on H3 and H5 was optimized to be 11:7.

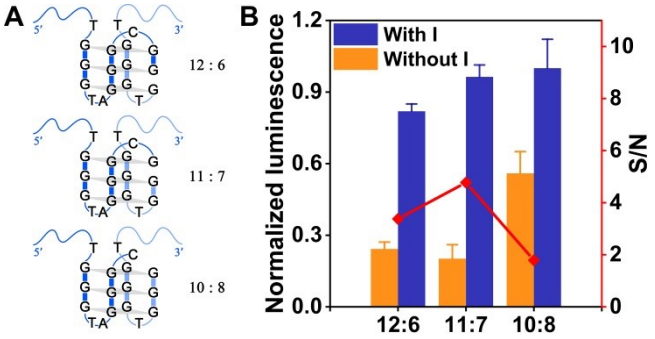

Fig. S13 (A) The schematic diagram of the split G-quadruplex mode of 12:6, 11:7, and 10:8 on H3 and H5. (B) The luminescence intensity of Ce6 corresponding to split G-quadruplex in different proportions.

Optimization of substrate concentration

Substrate concentration directly affects the luminescence intensity, so the concentration of the main reactants was optimized (**Fig. S14**). The intensity of the luminescent signal increased and then decreased with the increasing substrate concentrations, and the S/N value peaked with the concentrations of hemin, luminol, and H_2O_2 at 0.55 μM, 0.38 mM, and 0.16 M, respectively.

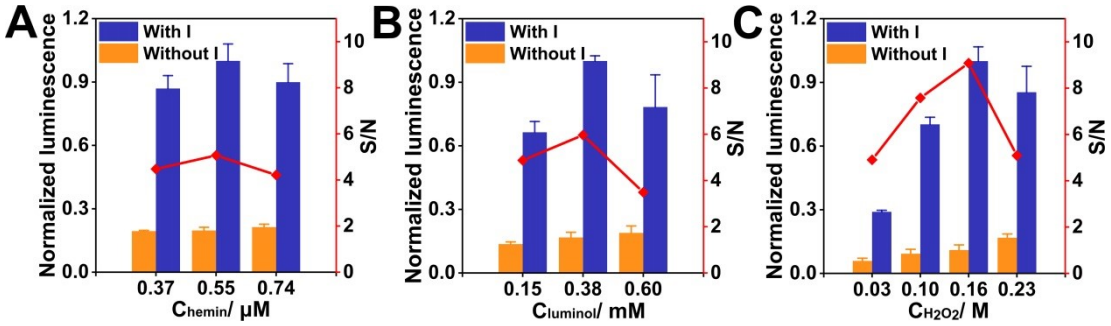

Fig. S14 Optimization of substrate concentration. (A) The Ce6 luminescence intensity and the signal-to-noise ratio of different concentrations of hemin. (B) The Ce6 luminescence intensity and the signal-to-noise ratio of different concentrations of luminol. (C) The Ce6 luminescence intensity and the signal-to-noise ratio of different concentrations of H_2O_2. The reaction was carried out in 10 mM HEPES buffer (pH 6.5, containing 600 mM NaCl, 50 mM KCl, and 10 mM $MgCl_2$). The concentration of hairpins H1-H6 in DNA incubation solution were 0.33 μM, 0.33 μM, 0.66 μM, 0.66 μM, 0.66 μM and 0.66 μM. Results are presented as means ± standard deviation (n = 3).

Detection of miRNAs by DCF signal readout

CRET-stimulated singlet oxygen was captured using a 2,7-dichlorodihydrofluorescein diacetate (DCFH-DA) probe by oxidizing non-fluorescent DCFH-DA to DCF with a fluorescence emission spectrum at 525 nm. The fluorescence of DCF increased linearly with increasing miRNA-21 concentration (**Fig. S15A**). A detection limit of 609.83 pM was acquired for miRNA-21 ($y = 19698 + 1049.9 * x$ with $R^2 = 0.98$). Significantly distinguishable detection of the target against several interfering nucleic acids, including miRNA-141, miRNA-222, and let-7a miRNA, confirmed the good selectivity of this circuit (**Fig. 15B**).

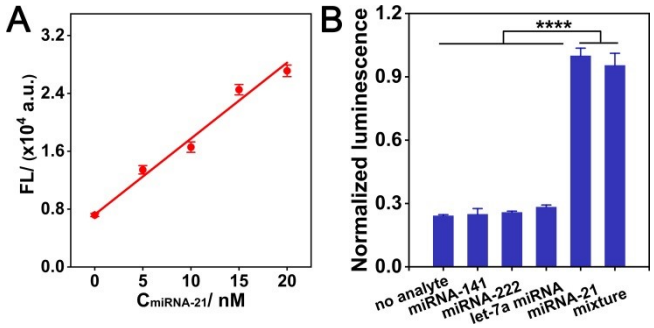

Fig. S15 (A) The fluorescence intensity of DCF has a linear relationship with different concentrations of miRNA-21. (B) The normalized DCF fluorescence intensity of the sensing system with different analytes (100 nM) for 12 h.

Cytotoxicity screening of different concentrations of hemin, luminol, and H_2O_2

MCF-7 cells were digested and counted, seeded into 96-well plates at a density of 1 × 10^5 cells/mL, and then placed in CO_2 culture for 24 h. Hemin, luminol, and H_2O_2 are diluted step by step into a series of concentration gradients. MCF-7 cells were incubated with different concentrations of substrates in a CO_2 incubator for 48 h. Then 20 μL of freshly prepared MTT solution (5 mg/mL) were added and co-cultured for 4 h. After the incubation, the cell culture medium was carefully removed from the 96-well plate, then 150 μL of dimethyl sulfoxide solution was added to each well, and they were shaken for 10 min at room temperature to mix well. Finally, the absorbance value (OD value) of each well at 490 nm was detected by a microplate reader from Tecan, Switzerland. Taking the blank group as a control, the relative cell viability values at different concentrations were calculated to screen the cytotoxicity of hemin, luminol, and H_2O_2, and they were optimized to be 200 nM, 250 μM, and 150 μM (**Fig. S16A, S16B and S16C**). The concentration of hydrogen peroxide in the intratumoral was about 100 μM-1 mM.[9,10] In addition, the DCF fluorescence intensity of the CHD circuit in solution was investigated with an H_2O_2 concentration of 250 μM and 1150 μM, which showed the obvious signal difference between the systems in the presence and absence of miRNA-21 (**Fig. S16D and S16E**). Therefore, 150 μM was selected as the optimal concentration of H_2O_2 in the subsequent cells experiments.

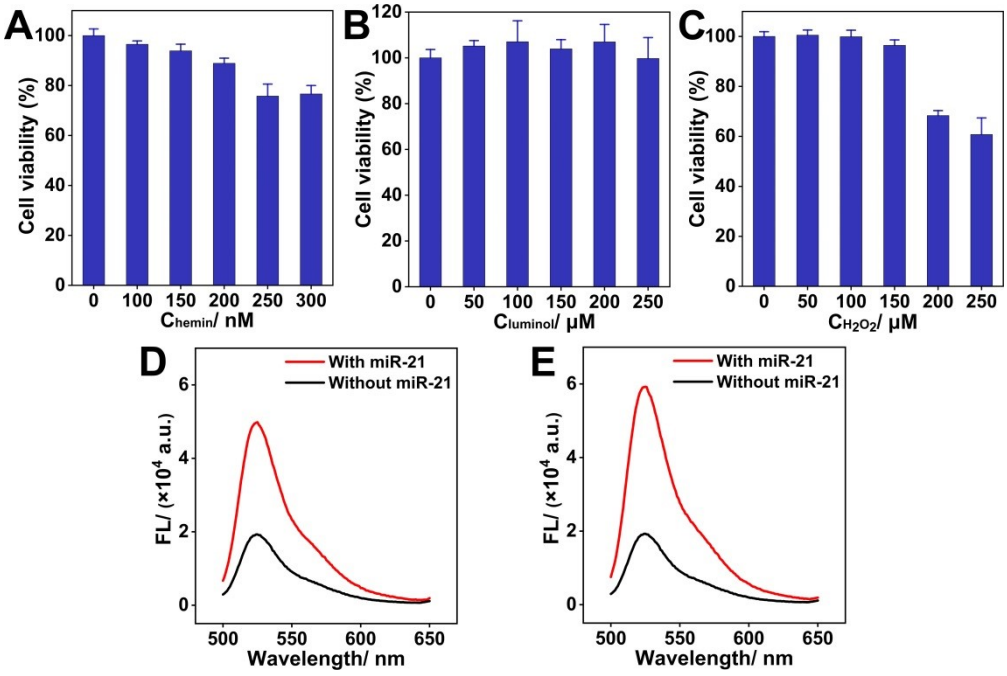

Fig. S16 (A) Cell viability of MCF-7 with different concentrations of hemin. (B) Cell viability of MCF-7 with different concentrations of luminol. (C) Cell viability of MCF-7 with different concentrations of H_2O_2. (D) Fluorescence spectra of DCF corresponding to the concentrations of H_2O_2 250 μM with miRNA-21 of 100 nM. (E) Fluorescence spectra of DCF corresponding to the concentrations of H_2O_2 1150 μM with miRNA-21 of 100 nM.

The cytotoxicity of the miRNA-initiated ROS

To demonstrate whether the miRNA-initiated ROS produces cytotoxicity, we verified it by MTT. The concentration of H_2O_2 is 150 μM (sample b). The CHA-HCR mixture containing H7* (0.025 nmol), H1* + H2* (0.3 nmol each), and H3* + H4* + H5* + H6* (0.6 nmol each)+hemin (200 nM)+luminuo (250 μM) are transfected into the cell (sample c). All of the components are transfected into the cells (sample d). As shown in **Fig. S17**, the miRNA-initiated ROS is weakly cytotoxic to cells. These results indicate that our system can be applied to the imaging of intracellular miRNA.

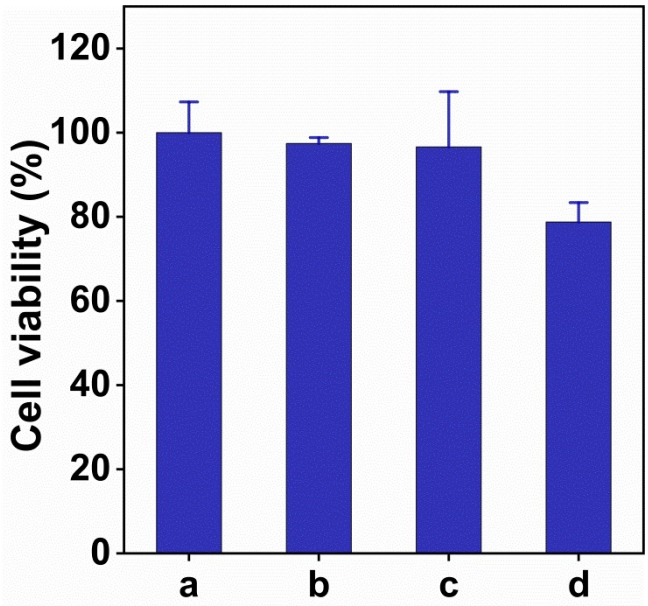

Fig. S17 The cytotoxicity of the ROS produced by miRNA-initiated CHD circuit. (a) PBS, (b) H_2O_2, (c) all hairpins + hemin + luminol, (d) all hairpins + hemin + luminol+ H_2O_2.

Optimization of liposome 3000 transfection DNA hairpin time

To prove that liposomes can transfect DNA hairpins into cells and optimize the time of liposome-transfected DNA hairpins, we selected hairpin H4 in the presence of Ce6 for verification. MCF-7 cells were digested and counted, seeded into six-well plates at a density of 5×10^5 cells/mL, and then placed in CO_2 culture for 24 h. Afterwards, hairpin Ce6-H4 (0.1 nmol) was transfected into the wells with serum-free medium (400 μl), and incubated with cells for 0 h, 2 h, 4 h, and 6 h. After the culture, the upper medium was discarded. Cells were rinsed 1-2 times with sterile PBS to remove excess medium. The cells in each well were then digested, collected by centrifugation, and dispersed into 1 mL of sterile PBS for use. Finally, the fluorescence intensity of Ce6 in cells at each incubation time point was collected and analyzed by the flow cytometer FACSVerse of BD Company in the United States. As shown in **Fig. S18**, the fluorescence intensity of Ce6 gradually increased and reached a plateau after 4 h, and 4 h was selected as the optimal transfection time.

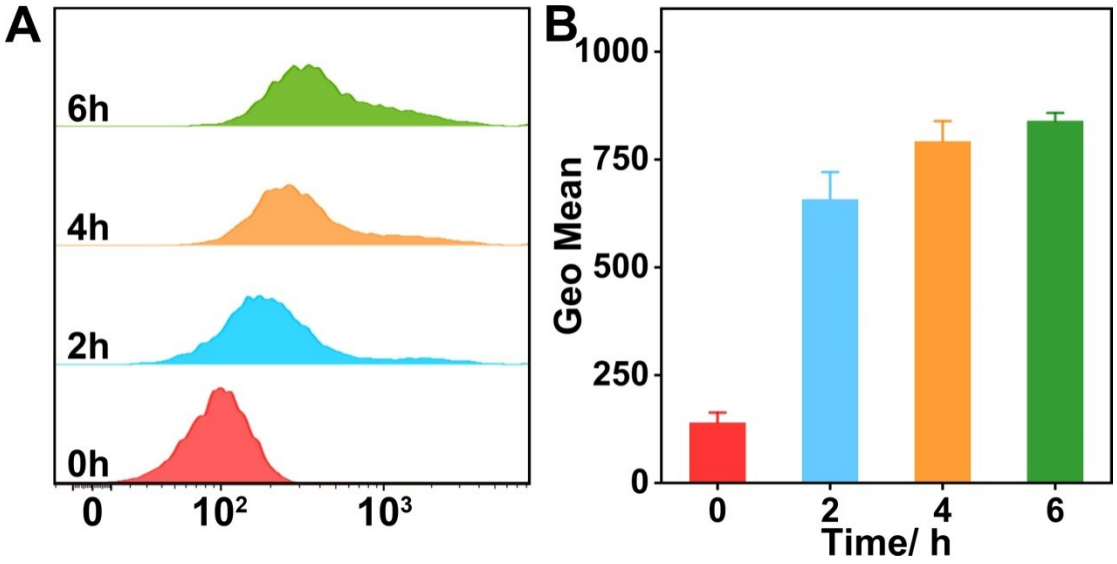

Fig. S18 Optimization of incubation time for hairpin Ce6-H4 in MCF-7 living cells. (A) Flow cytometric analysis and (B) the corresponding statistical fluorescence histogram analysis of Ce6-H4 transfected with liposome 3000 at different times at 37°C.

Effects of culture medium on hemin and luminol

The biostability of hemin and luminol in cell medium has been investigated by the UV spectrophotometer and chemiluminescence instrument. As shown in **Fig. S19**, the UV absorption of hemin, luminol chemiluminescence signal, and Ce6 luminescence signal maintained well for 4 hours, indicating the good biostability of these components.

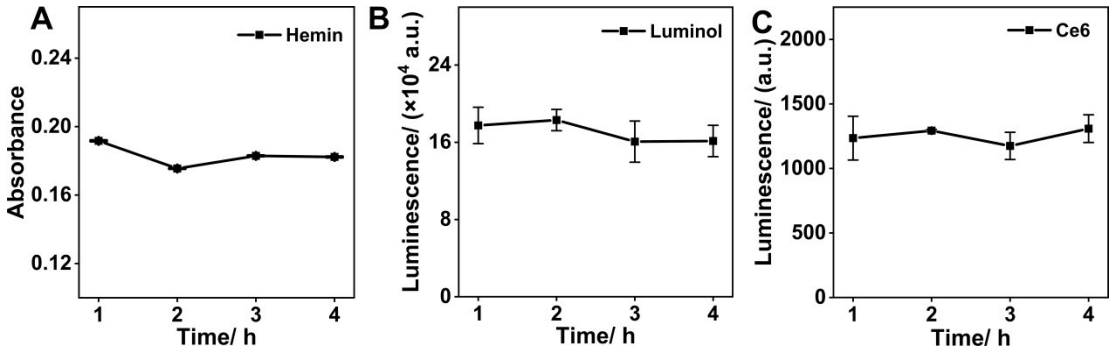

Fig. S19 (A) UV absorption of hemin in cell medium containing 10% serum for four hours. (B) Luminol luminescence in cell medium containing 10% serum for four hours. (C) Ce6 luminescence in cell medium containing 10% serum for four hours.

Optimization of DNA hairpin incubation time

The cellular uptake behavior of all DNA hairpins was investigated by flow cytometry. MCF-7 cells were digested and counted, seeded into six-well plates at a density of 5 × 10^5 cells/mL, and then placed in CO_2 culture for 24 h. Afterwards, H7* + H1* + H2* + H3* + H4* + H5* + H6* were transfected into the wells with serum-free medium, and incubated with cells for 0 h, 4 h, 8 h, 12 h, and 16 h. Then, DCFH-DA was added to the petri dish and cultured in the incubator for 30 min. Then, the dye was sucked out and washed once with serum-free medium 1640. Medium containing H_2O_2 was added and incubated for 5 min. With the increasing incubation time, the fluorescence of DCF reached a plateau after 12 h (**Fig. S20)**. Thus, 12 h was chosen as the optimized incubation time for the following experiments.

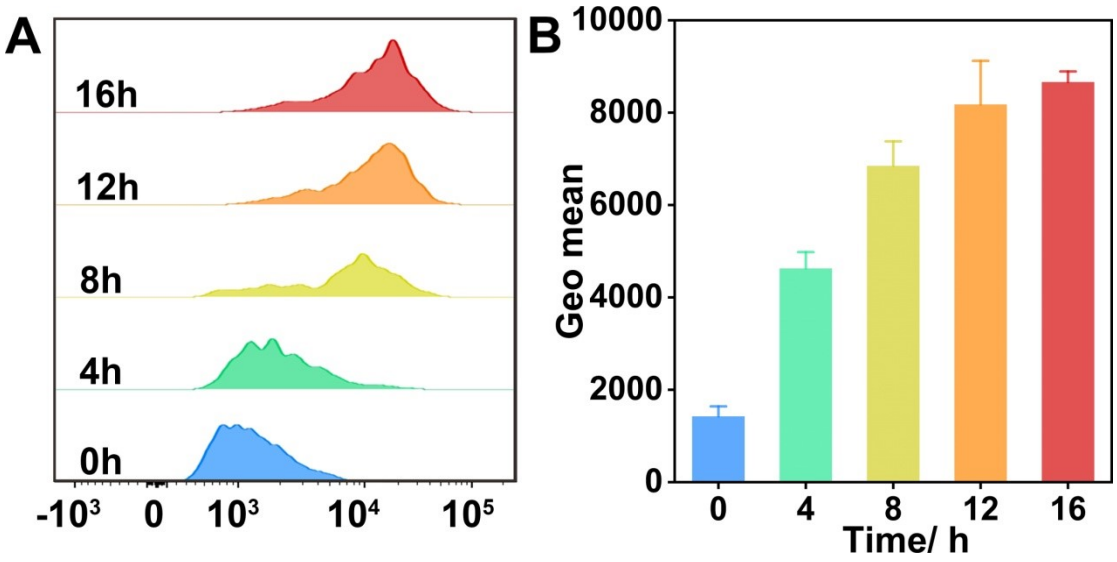

Fig. S20 Optimization of incubation time for the miR-21-targeting CHA-HCR-DNAzyme in MCF-7 living cells. (A) Flow cytometric analysis and (B) the corresponding statistical histogram analysis of CRET readout by incubating the CHA-HCR-DNAzyme with MCF-7 cells for different time-intervals at 37°C.

Imaging of intracellular DCF triggered by different contents of miRNA

Using DCFH-DA as a probe to monitor the ROS generated by the CHD circuit triggered by different miRNAs in cells. As shown in **Fig. S21**, the fluorescence of DCF with miRNA inhibitor (a) was almost ignorable. The fluorescent of DCF with miRNA mimic (c) is brighter than untreated (b). Statistical analysis of DCF fluorescence detected by flow cytometry was consistent with the CLSM results. The results suggest that the amplified fluorescent signal is attributed to miRNA-21-specific activation of the renewed CHD circuit.

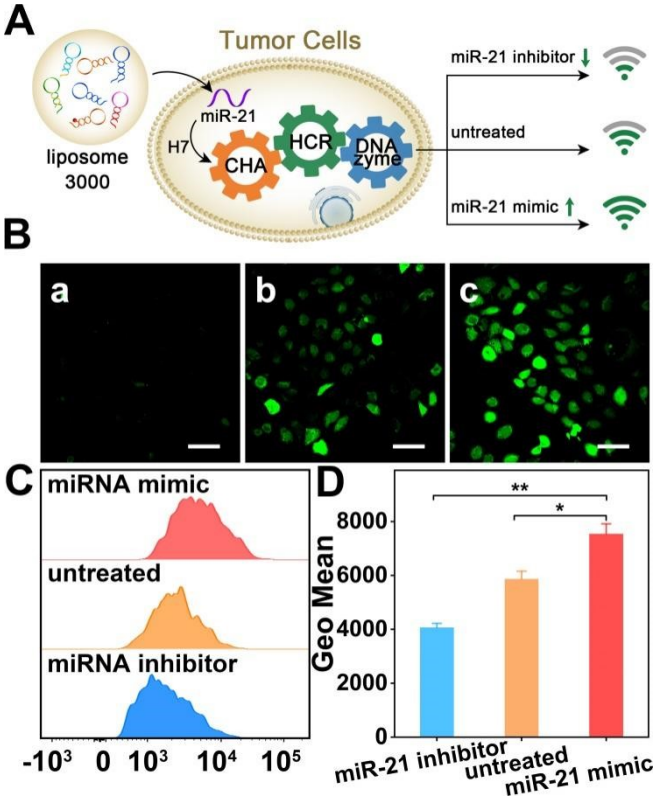

Fig. S21 (A) Schematic diagram of miRNA-21 detection was performed with miRNA inhibitor, untreated, and miRNA mimic based on the updated CHD circuit. (B) Intracellular miRNA imaging was performed with (a) miRNA inhibitor and (b) untreated (c) miRNA mimic, respectively. (C) Flow cytometry analysis of miRNAs in MCF-7 cells added with miRNA inhibitor, untreated, and miRNA mimic, respectively (scale bars: 100 μm). (D) Statistical analysis of fluorescence intensities in MCF-7 cells supplemented with miRNA inhibitor, untreated, and miRNA mimic, as shown in (B) (*$p < 0.05$, **$p < 0.01$, ***$p < 0.001$, ****$p < 0.0001$).

The qRT-PCR analysis of miRNA-21 in different cells

The relative expression level of miR-21 in MCF-7, HeLa, and MCF-10A cells were respectively evaluated by quantitative reverse transcription-PCR (qRT-PCR) assay. As shown in **Fig. S22**, the relative miR-21 expression level of MCF-7 is higher than that of HeLa, and the miR-21 content of HeLa is higher than that of MCF-10A, which is in good accordance with that of CHD detection (**Fig. 6**). Therefore, the designed CHA-HCR-DNAzyme (CHD) circuit based on chemiluminescent resonance energy transfer can distinguish the expression of tumor-associated miRNAs in different living cells and can be used to distinguish different cell lines.

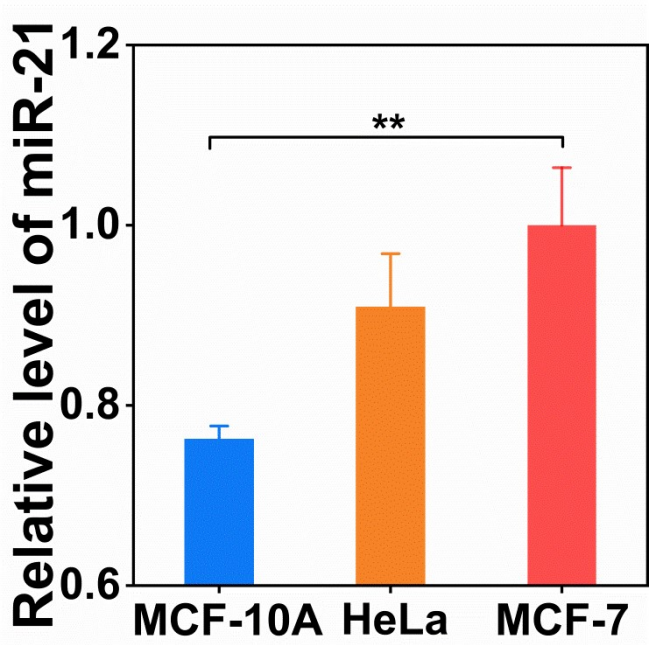

Fig. S22 The qRT-PCR analysis for the relative expression level of miRNA-21 in MCF-10A, HeLa, and MCF-7 cells, respectively. Results are presented as means ± standard deviation (n = 3) (*p < 0.05, **p < 0.01, ***p < 0.001, ****p < 0.0001).

References

1. P. Zhang, Y. Ouyang and I. Willner, *Chem. Sci*., 2021, **12**, 4810-4818.
2. J. Zhao, X. Jin, M. Vdovenko, L. Zhang, I. Y. Sakharov and S. Zhao, *Chem. Commun*., 2015, **51**, 11092-11095.
3. J. Li, T. Yuan, T. Yang, L. Xu, L. Zhang, L. Huang, W. Cheng and S. Ding, *Sens. Actuator B-Chem.*, 2018, **271**, 239-246.
4. Q. Wang, B. C. Yin and B. C. Ye, *Biosens. Bioelectron*., 2016, **80**, 366-372.
5. K. Saito, H. Tai, H. Hemmi, N. Kobayashi and Y. Yamamoto, *Inorg. Chem*., 2012, **51** 8168-8176.
6. Y. Cao, P. Ding, L. Yang, W. Li, Y. Luo, J. Wang and R. Pei, *Chem. Sci*., 2020, **11** 6896-6906.
7. T. Chang, H. Gong, P. Ding, X. Liu, W. Li, T. Bing, Z. Cao and D. Shangguan, *Chem. Eur. J.,* 2016, **22** 4015-4021.
8. A. Pertsinidis, Y. Zhang and S. Chu, *Nature*, 2010, **466** 647-651.
9. X. Qian, J. Zhang, Z. Gu and Y. Chen, *Biomaterials*, 2019, **211** 1-13.
10. F. Chen, P. An, L. Liu, Z. Gao, Y. Li, Y. Zhang, B. Sun and J. Zhou, *Nanoscale*, 2021, **13** 15677-15688.